



Statistical relationship between the succeeding solar flares detected by the *RHESSI* satellite

L. G. Balázs,^{1,2★} N. Gyenge,³ M. B. Korsós,³ T. Baranyi,³ E. Forgács-Dajka² and I. Ballai⁴

¹*Konkoly Observatory, Research Centre for Astronomy and Earth Sciences, Hungarian Academy of Sciences, Konkoly-Thege M. út 13-17, H-1121 Budapest, Hungary*

²*Eötvös University, Pázmány Péter sétány 1/A, H-1117 Budapest, Hungary*

³*Heliophysical Observatory, Research Centre for Astronomy and Earth Sciences, Hungarian Academy of Sciences, PO Box 30, H-4010 Debrecen, Hungary*

⁴*Solar Physics and Space Plasmas Research Centre (SP2RC), University of Sheffield, Hounsfield Road, Hicks Building, Sheffield S3 7RH, UK*

Accepted 2014 March 26. Received 2014 March 2; in original form 2014 January 14

ABSTRACT

The *Reuven Ramaty High Energy Solar Spectroscopic Imager* has observed more than 80 000 solar energetic events since its launch on 2002 February 12. Using this large sample of observed flares, we studied the spatiotemporal relationship between succeeding flares. Our results show that the statistical relationship between the temporal and spatial differences of succeeding flares can be described as a power law of the form $R(t) \sim t^p$ with $p = 0.327 \pm 0.007$. We discuss the possible interpretations of this result as a characteristic function of a supposed underlying physics. Different scenarios are considered to explain this relation, including the case where the connectivity between succeeding events is realized through a shock wave in the post Sedov–Taylor phase or where the spatial and temporal relationship between flares is supposed to be provided by an expanding flare area in the sub-diffusive regime. Furthermore, we cannot exclude the possibility that the physical process behind the statistical relationship is the reordering of the magnetic field by the flare or it is due to some unknown processes.

Key words: Sun: activity – Sun: flares – Sun: X-rays, gamma-rays.

1 INTRODUCTION

Sudden or explosive releases of energy are common phenomena in different cosmic objects occurring within a wide range of energy release rates from as low as 10^{17} J s^{-1} in the case of the Sun until as high as 10^{47} J s^{-1} in gamma-ray bursts at cosmological distances. In the present context, the notion of sudden or explosive event means that the ratio of the released energy (E) compared to rate of its change (dE/dt) is significantly shorter than the dynamical time-scale of the object, i.e. the ratio of the characteristic physical size (R) and the propagation speed (v) of any kind of disturbance initiated during the release (see, e.g. Wheeler 2012). A typical characteristic of these explosions is that the rising time of energy release is very short in comparison with the decay phase independently of the physics behind these explosions.

Our study will focus on sudden energy releases in the solar atmosphere called flares. The systematic multiwavelength study of flares revealed many details that help us in understanding the physics behind these phenomena; however, there are still many unanswered questions concerning the true dynamics and energetics of flares

(e.g. Priest & Forbes 2002; Shibata & Magara 2011; Fletcher et al. 2011). It is widely accepted that magnetohydrodynamic (MHD) processes are responsible for producing a flare. The energy released in a flare could originate from magnetic reconnection at the top of magnetic loop where the magnetic flux tubes take an X-type configuration. During reconnection events, the magnetic energy stored in magnetic field lines is released in a very localized way into thermal and kinetic energy. This energy is transported from the site of reconnection via, e.g. radiation, slow and fast MHD shock waves, accelerated particles and high-speed collimated hot plasma flows (jets). Flares usually occur in the solar corona but part of the released energy is transported downwards to the lower atmosphere where large-scale disturbances were observed travelling in a large distance away from the flaring sites as e.g. sunquakes observed in the photosphere (Kosovichev & Zharkova 1998; Moradi et al. 2007) or Moreton waves in the chromosphere (Moreton & Ramsey 1960). The energy of flares can be within a range of 10^{17} – 10^{26} J (Hannah et al. 2011).

Observations often reveal pairs of flares that occur with close temporal and/or spatial proximity and a physical connection between events was supposed to exist. Flares that occur because of common physical reason in different active regions (AR) are called sympathetic flares, and large-scale coronal structures are the most

★E-mail: balazs@konkoly.hu

probable causes of their connection (e.g. Moon et al. 2002; Török et al. 2011). Recently, Liu et al. (2009) found that four flares and two fast coronal mass ejections (CMEs) occurred with a causal relationship in an AR within ~ 1.5 h time interval. They called these types of solar flares occurring in the same AR with a causal relationship successive flares. Zuccarello et al. (2009) also found a sequence of successive destabilization of the magnetic field configuration starting with a filament eruption (relatively cool, dense object of chromospheric material suspended in the corona by magnetic fields) and ended in a large flare within ~ 2 h; they referred to the process as domino effect. Jiang et al. (2009) presented the evidence for occurrences of magnetic interactions between a jet, a filament and coronal loops during a complex event, in which two flares sequentially occurred at different positions of the same AR starting with 1 h time difference and two associated CMEs. Recently, Joshi et al. (2013) presented a study of a multiple flare activity containing three small flares, and a major eruptive flare over the period of two hours. They concluded that the small precursor flares (pre-flares) indicated the localized magnetic reconnections associated with different evolutionary stages of the filament in the pre-eruption phase and these events play a crucial role in destabilizing the filament leading to a large-scale eruption. The pre-flare activity occurs in the form of discrete, localized X-ray brightenings observed between 2 and 50 min before the impulsive phase of the flare and filament acceleration. Chifor et al. (2007) claim that the X-ray precursors provide evidence for a tether-cutting mechanism initially manifested as localized magnetic reconnection being a common trigger for both flare emission and filament eruption. Kim et al. (2008) also demonstrated that a pre-flare eruption and the main flare have a causal relation because they are triggered by a sequential tether-cutting process.

Based on these observations and conclusions, it is natural to question whether there are a significant number of flares physically connected in such way that their relationship can be revealed with statistical methods. This question is extensively debated in the literature but the statistical results presented so far have left this question open. The used methods usually focus on the study of flare waiting times distribution (WTD, the distribution of times between events) which can provide information about whether flares are independent events, or not (e.g. Wheatland 2000; Moon et al. 2002). The results suggests that the determination of WTD gives varied results, suggesting that the observed distribution may depend on the particular AR, on time, and that it may also be influenced by event definition and selection procedures (Wheatland 2009). The solar flare sympathy is probably a statistically weak effect (Wheatland & Craig 2006), but the successive flares probably do not occur randomly in time and the WTD are regulated by solar flare mechanisms (Kubo 2008). We apply an alternative statistical method that takes into account both the spatial and temporal distributions of flares.

The observational data used in the present study are the flares appearing in the list provided by the *Reuven Ramaty High Energy Solar Spectroscopic Imager (RHESSI)* satellite between 2002 and 2010. The paper is structured as follows: in Section 2, we present the observational set-up of our study and data used in the analysis. Section 3 deals with the statistical relationship between spatial and temporal differences of succeeding flares. The discussion on the possible physical interpretations of the statistical results is given in Section 4. Section 5 presents the summary of the main results and the conclusions. The paper includes an appendix containing a gallery of scatter plots for different time intervals displaying the statistical relationship discussed in the paper.

2 DATA USED IN THE ANALYSIS

2.1 RHESSI flare list

Since its launch, the *RHESSI* satellite (Lin et al. 2002) has observed more than 80 000 events in nine different energy channels. These events are displayed in a table consisting of the main parameters of flares (time of explosions, durations, peak intensities, total counts during the outburst, energy channel of the maximal energy at which the flare is still measurable, location on the solar disc and quality flags). The x , y positions of flares given in the *RHESSI* table refer to the apparent observed position of an event on the solar disc (Hurford et al. 2002). The flare position is the average of the map peak locations in different time intervals for the flare measured in the energy band from 6 to 12 keV. Based on this position, the number of the associated AR is determined and inserted into the flare list. *RHESSI* flares are mostly microflares of GOES class A, B or C; the most frequent type of flare being GOES class B. The thermal energy observed by *RHESSI* at the time of peak emission in 6–12 keV is in the range 10^{19} – 10^{23} J and has a median value of 10^{21} J (Christe et al. 2008; Hannah et al. 2008).

RHESSI microflares typically show elongated loop-like structures, which are interpreted as cooling post-flare loops. At first, the thermal hard X-ray (HXR) emission at the loop-top is seen in the lower energy bands. Later, the footpoints become visible in the higher bands because of the energy deposition of the non-thermal electrons penetrating to the loop footpoints. The hot material at the footpoints evaporates from the chromosphere to the corona to fill up the loop (Hannah et al. 2008, 2011), which can be seen as thermal loop source in the *RHESSI* images. The distribution of HXR (4–10 keV) source heights was found to be well fitted by an exponential distribution with a scaleheight of $6.1 \pm 0.3 \times 10^6$ m. The minimum observable height due to partially occulted sources was found to be $5.7 \pm 0.3 \times 10^6$ m in the solar corona (Christe, Krucker & Saint-Hilaire 2011).

2.2 Data processing and selection criteria

Our aim is to study the spatial and temporal relationship between *RHESSI* flares, thus we have to determine the spatial and temporal difference between two consecutive flares. The temporal difference was calculated by using the peak time of the flares. To derive spatial distances (m) between the locations of flares, at first we had to convert the x , y positions of flares (arcsec) to latitude and longitude (deg) of the Carrington heliographic coordinate system. During the orthographic projection transformation, we took into account the apparent variation of the solar rotation axis and radius because of orbital motion of the Earth. The height of flares should be also taken into account but the distance from the solar surface to the flares is not known. Therefore, we used the height of 6×10^6 m in each case, which is about that height where the flares are most frequently observed by *RHESSI* (Christe et al. 2011). After calculating the heliographic coordinates of flares, we computed their estimated spatial distance from their successors on a sphere with a radius of $R_{\odot} + 6 \times 10^6$ m. Obviously, the assumption for the height of flares inserts some systematic error in calculating the heliographic coordinates and the error of the position of flares increases with the increasing distance from the solar disc centre. To exclude the cases with relatively large errors, we have omitted all the events whose longitude measured from the central meridian (LCM) is greater than $\pm 60^{\circ}$. We also determined several selection criteria related to the AR where the flare occurred. At first,

Table 1. The number of events in different energy channels in the studied time interval (2002–2010).

Energy channel (keV)	All events	Selected events
6–12	38 058	15 132
12–25	9601	3431
25–50	902	294
50–100	116	46
100–300	53	26
300–800	8	4

we excluded those events that were not associated with an identified AR in the *RHESSI* flare list. In the remaining cases, the number of AR and the heliographic coordinates of flares were compared with the position data of AR available in the SOHO/MDI-Debrecen Data (SDD, 1996–2010) catalogue (Györi, Baranyi & Ludmány 2011). It was checked whether the position of flare and that of the AR in SDD can be matched with a tolerance limit of $\pm 10^\circ$ latitude and $\pm 20^\circ$ longitude. Finally, only those flares were selected which had the same identified AR both in SDD and in *RHESSI* flare list.

Further, some events were disregarded because of uncertainties of the observation of position or peak time. Each *RHESSI* orbit provides approximately 1 h of solar observations followed by about 40 min of time spent in eclipse. Solar observations are further reduced by passages through the South Atlantic Anomaly (SAA), during which the detector counts are not recorded due to the high flux of energetic particles (Christe et al. 2008). To avoid using flares with misidentified peak times, we disregarded events that occurred during passing into the Earth’s shadow or during data gap, or which were connected to the entering phase of the satellite above the SAA. We also omitted from further considerations the events with invalid position data.

We also considered the energy channel of the maximal energy at which the flare is still measurable regardless of the energy channel of its successor. The flares in the energy channel 6–12 keV have enough number for statistical studies in different phases of the solar cycle; thus, we have confined our analysis to these types of events. Table 1 shows the number of the events in the flare list and the number of the events meeting our selection criteria in various energy channels in the studied time interval (2002–2010).

3 STATISTICAL RELATIONSHIP BETWEEN SUCCEEDING FLARES

In order to study the statistical relationship between succeeding flares, we computed their spatial (ds) and temporal (dT) difference, i.e. the spatial and temporal distance of succeeding flares. We grouped the flare events according to the phase of the solar cycle to ensure equal number of considered cases. In this way, we selected 6 sub-samples in the 6–12 keV energy channel.

At first, the ds and dT values were displayed in scatter plots based on the flares in the 6–12 keV energy channel without selecting out the succeeding flares in different AR as it can be seen in Fig. 1. A correlation between the measured quantities for succeeding flares would mean some sort of casual relationship between them. In this figure, the data points populate two major branches divided by a ‘valley’ at about $ds = 10^8$ m. The points above 10^8 m do not show any relationship with the dT time difference, i.e. there is no relationship between the flare and its successor in these cases.

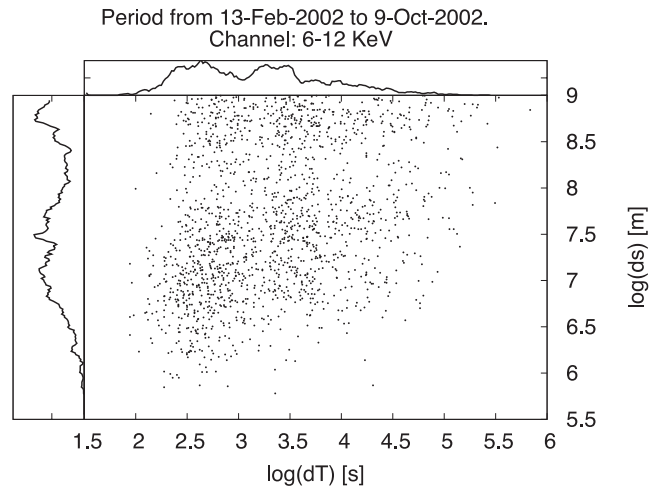


Figure 1. The distribution of succeeding flares in the $\{\log_{10}(ds); \log_{10}(dT)\}$ plane. Note the two major populations of the events divided by a horizontal ‘valley’ at about 10^8 m. The rising trend in the lower population of events may indicate some relationship between the temporal and spatial differences of succeeding flares.

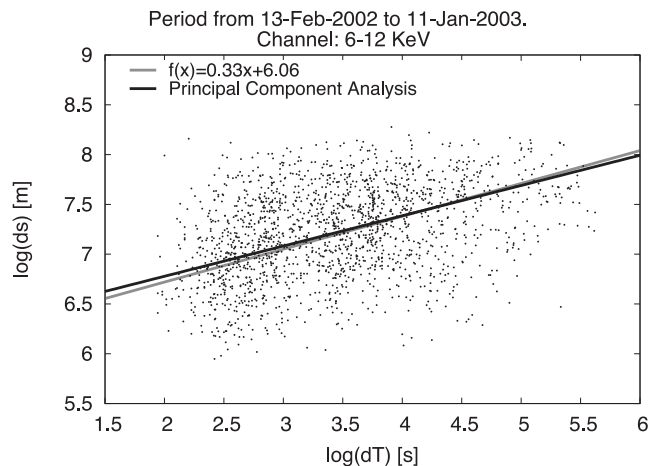


Figure 2. Distribution of flares in the 6–12 keV channel and their successors in the $\{\log_{10}(ds); \log_{10}(dT)\}$ plane. The black solid line indicates the actual result of the PCA regression and the grey line is determined by the average parameters of Table 2.

In contrast, the points below the ‘valley’ populate a ridge having a well-defined rising tendency with ds as the time difference is increasing between two succeeding flare events. This rising tendency might be interpreted as a possible causal relationship between succeeding flares.

Fig. 1 also shows vertical strips containing more and less number of points in reflecting the orbital motion of the *RHESSI* satellite around the Earth with maximum of points at about the orbital period of *RHESSI* (96 min) and with minimum of points at about 38 min because of the time spent in the Earth’s shadow.

Considering only the succeeding flares in the same AR, the population of points above $ds = 10^8$ m disappears and only the cases representing the rising trend remain (see Fig. 2).

To characterize the rising trend in the $\log_{10}(ds) \log_{10}(dT)$ diagram, we assume that the measured quantities can be written as $\log_{10}(ds) = \log_{10}(R) + \varepsilon_s$ and $\log_{10}(dT) = \log_{10}(t) + \varepsilon_t$, where R and t are the true distance and time differences between two flares

Table 2. Parameters in equations (2) and (3) obtained from the PCA regression for the flares in the 6–12 keV energy channel.

Start date	End date	a	b	St.Dev. (a)	St.Dev. (b)
2002-02-13	2003-01-11	0.304	6.170	0.017	0.087
2003-01-11	2003-08-04	0.336	6.026	0.017	0.090
2003-08-04	2004-04-20	0.350	5.991	0.019	0.101
2004-04-20	2005-01-13	0.350	6.025	0.021	0.100
2005-01-13	2006-04-26	0.304	6.137	0.019	0.091
2006-04-26	2010-12-31	0.317	6.019	0.016	0.088
Average		0.327	6.061	0.007	0.038
2002-02-13	2010-12-31	0.324	6.072	0.007	0.037

and ε_s , ε_t represent noise terms. We represent the rising trend as a $\log_{10}(R) = p \log_{10}(t) + b$ linear relationship corresponding to an equation of the form

$$R(t) = At^p. \quad (1)$$

The supposed relationship between the observed variables, ds , dT , can be expressed by a linear regression model between the logarithmic variables:

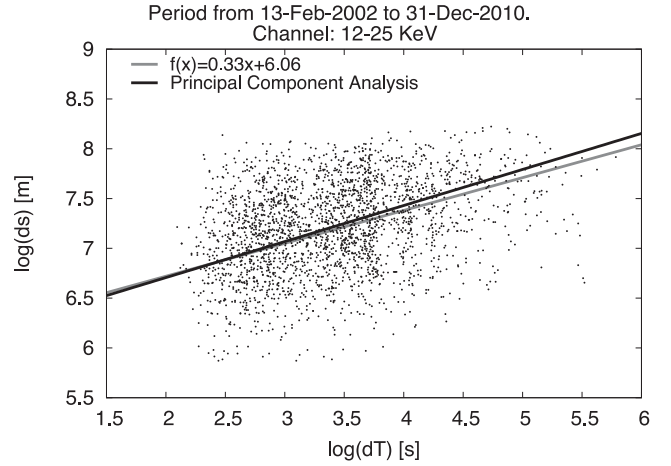
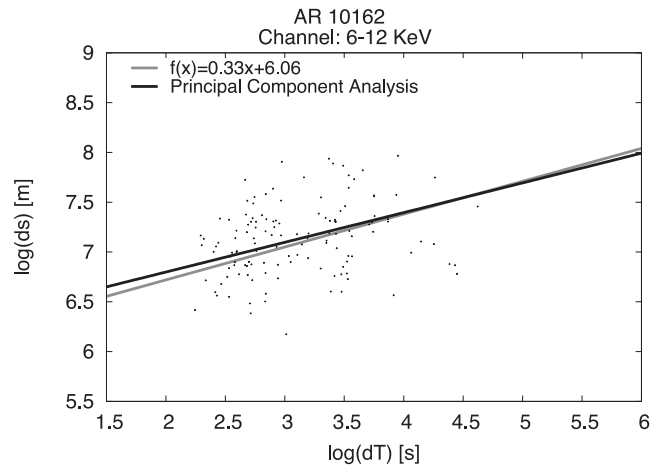
$$\log_{10}(ds) = a \log_{10}(t) + b + \varepsilon_s \quad (2)$$

$$\log_{10}(dT) = \log_{10}(t) + \varepsilon_t, \quad (3)$$

where $a = p$ and $b = \log_{10}(A)$. The default procedure for the verification of the factor model is usually the principal component analysis (PCA; see e.g. Cadavid, Lawrence & Ruzmaikin 2008) performed on the covariance matrix of the $\log_{10}(ds)$, $\log_{10}(dT)$ variables. Performing the PCA and keeping the first PC, we obtain a variable running along the maximal variance direction of the points in the $\{\log_{10}(ds); \log_{10}(dT)\}$ plane. The regression line obtained in this way minimizes the sum of quadratic distances of the data points to a line. Therefore, this kind of regression is also called orthogonal, and it gives the values of parameters a and b in the above system of equations. The obtained parameters are summarized in the Table 2. The errors in our estimations were calculated by means of the orthogonal regression (see, e.g. Isobe et al. 1990).

The observed successor of a flare is not necessarily the true one because, e.g. it can be below the detection limit or in a phase when the satellite is not active (the instrument is in the SAA or in the Earth shadow). One may have a concern, therefore, that this circumstance inserts some bias on the estimated parameters. For testing the effect of missing data on the statistical result, we created a sub-set of the data by leaving out a large number of the observed events. We selected only those events that were observed in the 12–25 keV channel and the result can be seen in Fig. 3), which shows that the pattern does not depend on whether the observed successor of a flare is really the true one. Thus, we can conclude that the statistical result is not or hardly sensitive to the data missing for any reasons.

The robustness of our approach can be also tested by using the flares in one AR. We have chosen the active region AR 10162 as a representative sample that contained 253 events recorded in the period 2002 October 17–31, giving us a good basis for statistical investigation. Performing the same analysis as before (PCA), we arrive to a similar pattern (see Fig. 4) as derived earlier for the full *RHESSI* data base. For this particular AR,

**Figure 3.** Distribution of succeeding flares in the $\{\log_{10}(ds); \log_{10}(dT)\}$ plane in the 12–25 keV channel. The meaning of the lines is the same as in Fig. 2.**Figure 4.** Distribution of succeeding flares in the $\{\log_{10}(ds); \log_{10}(dT)\}$ plane in the 6–12 keV channel for the active region AR 10162. The meaning of the lines is the same as in Fig. 2.

we obtained that the parameters describing the fitting line are $p = 0.3$ and $b = 6.2$.

4 DISCUSSION ON THE PHYSICAL INTERPRETATIONS

4.1 Sedov–Taylor blast wave

Table 2 shows that the mean value of the parameter p (the power of the relationship between R and t) resulting from the fitting line shown in Figs 2 and 3 is $a = p = 0.327 \pm 0.007$. Based on this finding, we will try to explain the relationship between the spatial and temporal differences between events assuming that it reflects a physical relationship.

The first thing we can notice is that of all the p values determined above are close to the value of $p \sim 1/3$ typical for blast waves in the post-Sedov–Taylor phase. The fast-mode freely propagating blast waves are a common feature of many flare models, and the reconnection model, that stays at the core of flaring processes, describes two additional types of shocks (slow-mode Petschek shocks

and fast-mode termination shock), which can have an impact on the ambient medium (see, e.g. Forbes 1988).

The energy release of flares would always act as a temporary piston for a shock that propagates later as a pressure-driven blast wave (see the review by Vrřnak & Cliver 2008). Shocks can be also ignited by a smaller scale process associated with the flare energy release, e.g. expansion of hot loops or small-scale ejecta. Numerical simulations show that other alternative mechanisms may be available; e.g. the downward reconnection jet (which may or may not be supersonic) might create a large-scale fast-mode shock wave in the ambient corona after coalescing with the low-lying loops and deforming them (Bárta, Vrřnak & Karlický 2008).

CMEs can also create coronal shocks but this type of shocks propagates in a different way. The magnetically driven CME creates a shock which is a combination of the bow-shock and piston-shock, and the wave is permanently supplied by the energy from the CME. These CME-driven shocks can later degenerate into large-scale global EIT/EIV waves (see, e.g. Ballai, Erdélyi & Pintér 2005) that can generate oscillations of various remote magnetic structures. Although blast waves at the onset of energetic flares are theoretically predicted, in most of the observations the coronal shock is related to CMEs or CME/flare events. So far there have been found only a few events that demonstrate that the coronal shock wave can be generated by a flare without the presence of an associated CME (Magdalenic et al. 2012; Kumar & Innes 2013). In addition, it is most likely that real shock waves are neither purely blast waves nor purely piston ones (Grechnev et al. 2011). Some further considerations may arise when we take into account the favoured place of formation of blast wave. Both theoretical models and observational results are in agreement in that only flares extending to the AR periphery are likely to ignite large-scale blast wave because strong field regions are unfavourable for generation of flare-associated pressure pulses (Vrřnak & Cliver 2008). However, our results could only be explained in terms of blast waves if there were pieces of observational evidence for the existence of such flare-ignited small-scale disturbances which can propagate within the AR as a blast wave at least in a part of their propagation time. Despite the lack of such pieces of observational evidence, it is reasonable to investigate whether our results support or refute the existence of such blast waves that could cause the determined statistical relationship.

The process of explosive energy release can generate a radially expanding shock wave in a homogeneous surrounding medium described by the Sedov–Taylor theory (Sedov 1946; Taylor 1950). After the explosion, the shock wave enters into an adiabatic expansion phase corresponding to a power law of the form given by equation (1) with $p = 0.4$. The coefficient A is related to the ratio of the inputted energy, E , of the blast wave and the ambient density, ρ , via the equation

$$A = \left(\frac{E}{\rho B(\gamma)} \right)^{1/5}, \quad (4)$$

where the constant $B(\gamma)$ depends only on the specific heat ratio, γ . In the case of $\gamma = 5/3$ one obtains $B(\gamma) \approx 1$.

Later on, the shock wave enters the post-Sedov–Taylor expansion phase, when the characteristic time of the energy loss is comparable to the characteristic time of expansion of the shell. The pressure of hot shocked gas can still drive a shock into the surrounding medium, but radiation losses become important. When the shell has expanded and decelerated sufficiently so that its cooling time is shorter than its spreading time, it loses energy rapidly by cooling. Due to the gradual loss of the intrinsic energy of the wave, the power p drops down to about 1/3. In the stage of pressure-driven

snowplow (PDS), the analytic value of p is $2/7 = 0.286$ (McKee & Ostriker 1977). The numerical simulations of the transition of the Sedov–Taylor blast wave from adiabatic to PDS derive somewhat higher values of p varying in time and depending on the numerous characteristics of the ambient medium. For example, the power p is expected to be about 0.31 (0.300–0.320) by Chevalier (1974) or about 0.33 (0.312–0.342) by Blondin et al. (1998) in the case of thin-shell radiative blast wave. The final stage is a momentum-conserving phase corresponding to a power $p = 0.25$ (Tenorio-Tagle & Bodenheimer 1988).

Our statistical method suggests that the relationship between successive flares could follow the propagation characteristic of a shock wave in post-Sedov–Taylor phase. The result is independent of the fact that we see only the projected distance of two spatially separated events on to the plane perpendicular to the line of sight. From statistical point of view, the events distributed uniformly on a sphere of radius $R(t)$ populate, as a projection, a ring with approximately the same outer radius. Consequently, the relationship between the time and distance of two succeeding flares remains unchanged. Thus, our statistical results may allow us to reveal the basic properties of the determined relationship assuming that it describes a physically existent blast wave.

4.2 Parameter estimation for the blast wave

The constants b derived by means of the PCA regression impose a constraint upon the value of A . The fitting with the help of equations (2) and (3) results in a range of values of $b = \log_{10}(A) = 6.02\text{--}6.10$, i.e. $b = 6.06 \pm 0.04$ as given in Table 2.

Computing the time derivative of the shock front radius, $R(t)$, we obtain the velocity of the propagating shock pattern as

$$v_R = \frac{dR(t)}{dt} = pAt^{p-1} = p \frac{R(t)}{t}. \quad (5)$$

Estimating the inputted energy, the density of the various layers of the solar atmosphere and the local magnetoacoustic speed, we can investigate whether a blast wave with the obtained values of A can propagate in that medium.

Flares could occur in the solar corona, and it is known that the magnetic reconnection, which stays at the core of flare generation, can drive fast shock waves in their surroundings. At first, we discuss the simplest and the most obvious scenario to explain the connectivity of events is that the blast wave is generated at the location of the first flare and it propagates on the disc in the solar corona until it triggers a subsequent reconnection in the same AR.

Considering the typical density in a coronal AR of the order of $10^{-12}\text{--}10^{-13} \text{ kg m}^{-3}$ (Aschwanden 2005) and using the value of $b = \log_{10}(A)$, we can derive a range of energies of $10^{17}\text{--}10^{19} \text{ J}$. We have to note that this estimation has a certain level of uncertainty that could result from the estimations of density and constant A . The estimation of the density of the ambient medium is not an easy task. The density is measured from emission lines, but when looking at the emission in a certain wavelength one has to consider the effect of all origins of emissions in the line of sight, therefore estimates of densities might be overestimated. The constant $B(\gamma)$ is not affecting the determined energy values as its value depending on the specific heat varies within a very narrow interval.

We should note that this energy is not necessarily the entire energy released by the flare and not even the whole resulting kinetic energy. The thermal and kinetic energies are not necessarily equal, and the equipartition rule between them is not known. Thus, the thermal energy of flares can be used as an estimated upper limit of energy

of the shock wave. Taking into account that the thermal energy of microflares is 10^{19} – 10^{23} J, we can estimate that a microflare usually has enough energy to generate a shock wave with $A \sim 10^{6.02}$ – $10^{6.10}$ in the solar corona but hardly or not at all in the denser lower atmosphere. Now the question is whether such a shock wave can propagate in the solar corona.

The uncertainty in calculating the coefficient A does not affect the estimation of the velocity of the shock pattern. One can see from equation (5) that the right-hand side does not depend on the constant A and consequently on the uncertainties mentioned above.

For calculating the range of propagation speeds, v_R , we need the value of the time parameter, t , appearing in equation (5). However, this parameter is a hidden variable in equations (2) and (3) due to noise and is not accessible directly from observations, nevertheless it can be calculated from the observed dT time differences.

Inspecting the figures listed in the appendix, one can obtain an estimate for the observed time difference to be in the range $2 < \log_{10}(dT) < 5.5$. According to the PCA method, the hidden time variable, t , accounts for about 0.7 of the variability of the observed value. Consequently, the range of the parameter $\log_{10}(t)$ is $2.5 < \log_{10}(t) < 5$.

Converting these values to those of the velocity of the shock we obtain a range of $0.13 \text{ km s}^{-1} < v_R < 6.7 \text{ km s}^{-1}$. If the connection between events is realized by a propagating shock wave, this can only propagate in a region where the propagation speed of the shock front exceeds the local speed of linear fast magnetoacoustic waves. This speed is of the order of several hundred km s^{-1} in the solar corona and it is about 10 km s^{-1} in the photosphere. This means that the derived speed is completely unrealistic for a shock wave propagating in the solar corona or even in the photosphere. Consequently, we obtain a contradiction by assuming a direct blast wave connecting two succeeding flare events; therefore, alternative explanations that could shed light on the very low propagation speed are needed.

We have three possible ways which can be investigated whether they help to resolve this problem: (1) the parameter estimation for the Sedov–Taylor equation needs improvement; (2) the blast wave propagates only in a fraction of the observed time; (3) the real physical connection between flares is not a blast wave.

The first possible explanation for the above contradiction is that the direct blast wave propagates in the corona but its estimated speed is not correct. This could arise because our model lacks the influence of the magnetic field, which may preclude the correct parameter estimation. In an AR, the dynamics is driven by magnetic forces which can alter equation (4). However, this simplification cannot explain why the derived propagation speed is smaller by several order of magnitude than the local speed of linear fast magnetoacoustic waves in the corona.

The second possible way to resolve the problem is to assume that the blast wave is only a part of a sequence of the dynamic events generated by the instigator flare. If the time for the disturbance to propagate in form of a blast wave is only a fraction of the elapsed time we observed between two succeeding flares, the propagation speed of the blast wave can be larger than the speed determined for the whole time. However, one order of magnitude increase in speed of blast wave would need five orders of magnitude increase in energy of flare. Since the speed would need about four orders of magnitude increase, thus we have to conclude that the microflares probably cannot generate such a Sedov–Taylor blast wave propagating in the solar corona that could explain the results presented in this paper.

If we assume that the disturbance propagates in form of a blast wave only in a fraction of both the total spatial and temporal distances, it may formally resolve the problem. The available energy can be enough for a blast wave to propagate a small fraction of the spatial difference with an appropriately high speed in a fraction of the elapsed time. However, in this case, the equations would contain more unknown parameters than that could not be determined by using the present method because we do not know how the disturbance propagates in the remaining part of its propagation and what else happens during the remaining part of the time interval. We can only discuss the known models, observations, and simulations whether they allow such a scenario.

According to the standard flare model, the flare taking place in the corona can generate energetic disturbances that can travel towards the footpoints in the denser lower atmosphere. These disturbances arriving in the chromosphere or the photosphere can trigger blast waves. If we assume that such a type of blast waves plays a role in the found relationship, it allows the blast wave to propagate only a part of the observed distance in a part of the observed time. It is reasonable to assume that a blast wave propagating in the photosphere can collide with a neighbouring flux tube triggering a disturbance propagating upwards, eventually leading to a succeeding flare. In this scenario, the observed time consists of three different time intervals. The first one is the travel time of transporting the energy from the location of the flare to the triggering site of the blast wave. The second one is the time the blast wave spends in-between its origin and the footpoint of the neighbouring flux tube and finally, the time necessary for a secondary disturbance to reach the location of the succeeding flare event from the place where the blast wave collided with the magnetic flux tube.

The triggering disturbance for the subsequent flare is probably a plasma upward flow according to the simulation by Sakai et al. (2000). These authors studied the process of interaction between shock waves and magnetic flux tubes taking into account the effect of the gravitationally stratified background density, and they found that a strong upward plasma jet, as well as surface Alfvén waves can propagate along the flux tube. The shock wave travelling to a current sheet may initiate magnetic reconnection process according to the simulations by Odstrčil & Karlický (1997), which supports the idea that the solar flare can be triggered by the shock wave coming from a distant flare.

This scenario is also supported by the observation of Moretti et al. (2003). They found a triggering strong plasma upward flow before a B-class flare and after a few minutes, an impulsive event was detected at chromospheric heights. About 10 min later, they observed downward plasma pulses with energies of the order of 10^{18} – 10^{19} J penetrating down to the photospheric layers, and they observed 11 similar downflows during 47 min all together. The duration of the impulses was always of the order of 510 min, and they caused shock waves in the photosphere with an initial horizontal propagation speed of about 20 km s^{-1} . By using the real energy of flares, we can estimate the range of $\log_{10}(A)$ to be between 4.8 and 5.4 in similar cases. If the $\log_{10}(A)$ is in this range, the shock front can be estimated to propagate horizontally a distance of about 100–600 km within a few seconds. If the shock wave collides with a flux tube during this propagation, this may result in a flare later according to the above mentioned simulations by Sakai et al. (2000) and Odstrčil & Karlický (1997). Based on these results, it seems possible that a flare-generated shock wave can contribute to the generation of a next flare in such a way. However, it cannot be decided now whether the outlined scenario works or not.

4.3 Other possible physical interpretations

It is also possible that the connection between the succeeding flares is not even realized by a shock wave but by an unknown physical mechanisms, whose kinematic characteristics resemble the properties of a blast wave. In a recent paper, Aschwanden (2012) investigated 155 M- and X-class flare events seen by GOES and SDO/AIA satellites and measured the spatial and temporal expansion of flare areas. His main finding was that for the majority of the cases the expansion was sub-diffusive with the expansion rule obeying the relation $r(t) \sim t^{\beta/2}$, where $\beta = 0.53 \pm 0.27$ that could be attributed to the anisotropic chain reactions of intermittent magnetic reconnection episodes in a low plasma-beta corona. The speed of area propagation was of the order of $15 \pm 12 \text{ km s}^{-1}$, a value that cannot be explained in terms of MHD waves. Despite the extremely large error resulted in his statistics (≈ 50 per cent), the value of $\beta/2$ is very close to the value we obtained by fitting a much larger sample of *RHESSI* data. Based on this model, we can imagine that the area of a flare in its expansion triggers subsequent flares in the same AR.

During a flare, the change of the magnetic structure in the corona is reflected in the motion of chromospheric H α flare ribbons and corresponding HXR footpoint sources. It is often observed by *RHESSI* that the source of HXR flux has a spatial displacement along the arcade of magnetic loops during a flare. This could be caused by some disturbance propagating along the arcade, sequentially triggering a reconnection process in successive loops of the arcade (e.g. Grigis & Benz 2005; Yang et al. 2009). These consecutive flaring events identified from a single flare may be observed as successive flares as they produce separate HXR peaks. The mean velocity of the footpoint motion determined by Inglis & Dennis (2012) is about $5\text{--}70 \text{ km s}^{-1}$ which is of the same order of magnitude as the propagation speed derived from our results in the time range between a few seconds and a few minutes. Thus, it is reasonable to assume that the above-mentioned features may contribute to the found statistical relationship in the time range of duration of flares. On the times scales of hours and days, the evolution of AR probably has a large contribution to the change of the position of flaring sites or dominates it.

Finally, our results could be a signature of a much intricate physics connected to the reorganization of the magnetic field following a flare. Flares always occur at the boundary of large neighbouring patches with opposite vertical magnetic field. When these fields are pushed together, reconnection takes place and a huge amount of energy is released. Flares are observed to take place where the magnetic field has a strong distorted configuration (twist of shear), meaning that the only way to release the magnetic helicity stored in magnetic field lines is through the eruption. These events are followed by a large-scale reorganization of the magnetic field whose kinematic parameters would follow the relationship we found earlier.

5 SUMMARY AND CONCLUSIONS

In this paper, we studied the statistical relationship between succeeding flare events recorded by the *RHESSI* satellite. We selected the flares that were associated with AR in the period 2002–2010.

The heliographic coordinates of events were calculated applying the appropriate corrections. With the help of the coordinates, we were able to determine spatial distances between succeeding events (ds) in the same AR, while temporal differences (dT) were deduced from the *RHESSI* catalogue.

We studied the statistical relationship between the ds and dT differences dividing the *RHESSI* data in sub-samples according to the phase of the solar cycle and the energy channels, respectively.

If we take into account only flares occurring in the same AR, we obtain a linear relationship in the $\{\log_{10}(ds) - \log_{10}(dT)\}$ diagram indicating a power-law connection between the spatial and temporal differences of succeeding flares.

This relationship may reveal a hidden factor responsible for the statistical connection. Performing a PCA on the ds and dT values, we obtained the parameters of the power-law relationship. The parameters obtained in this way showed a remarkable homogeneity, independently from the phase of the solar cycle.

Several possibilities were discussed to explain the temporal and spatial correlation between events. One candidate that could explain the connectivity was a blast wave. This assumption was made based on the statistically determined time-distance relationship of the form $R(t) = At^p$, where $p = 0.327 \pm 0.007$, i.e. very close to the typical value of a shock in the post-Sedov–Taylor stage. The most problematic point of this scenario is the derived propagation speed of these shocks being sub-sonic, at least a few orders of magnitude less than expected. We had to assume that the blast wave transmitting the causal connection between two succeeding flares takes only a few percent of their spatial and temporal differences if it plays a role at all.

It seems more possible, that the net effect of different, basically magnetic, processes in the solar atmosphere mimics statistically a functional relationship between the time and spatial distances of succeeding flares in a mathematical form of a blast wave. In particular, the relationship between temporal and spatial distances we observed could be the characteristics of the magnetic field re-arrangement after a flare in the same AR.

Finally, we need to note that our derived values are similar to the values obtained earlier by Aschwanden (2012) using SDO data, where the spatial and temporal differences were connected to the expansion of the AR area in the sub-diffusive stage. If our data analysis would point to the same mechanism described by this author, it would be a further evidence for the universal character of it as, according to our findings, this occurs not only in particular AR but it can be shown to be a trend over much longer periods.

ACKNOWLEDGEMENTS

This work was supported by the OTKA grants no. K77795, K81421 and K83133. The research leading to these results has received funding from the European Community's Seventh Framework Programme (FP7/2007-2013) under grant agreement eHEROES (project no. 284461).

REFERENCES

- Aschwanden M. J., 2005, *Physics of the Solar Corona. An Introduction with Problems and Solutions*. Praxis Publishing Ltd, Chichester
- Aschwanden M., 2012, *ApJ*, 757, 94
- Ballai I., Erdélyi R., Pintér B., 2005, *ApJ*, 633, 145
- Bárta M., Vršnak B., Karlický M., 2008, *ApJ*, 477, 649
- Blondin J. M., Wright E. B., Borkowski K. J., Reynolds S. P., 1998, *ApJ*, 500, 342
- Chevalier R. A., 1974, *ApJ*, 188, 501
- Cadavid A. C., Lawrence J. K., Ruzmaikin A., 2008, *Sol. Phys.*, 248, 247
- Chifor C., Tripathi D., Mason H. E., Dennis B. R., 2007, *A&A*, 472, 967

- Christe S., Hannah I. G., Krucker S., McTiernan J., Lin R. P., 2008, *ApJ*, 677, 1385
- Christe S., Krucker S., Saint-Hilaire P., 2011, *Sol. Phys.*, 270, 493
- Deeming T. J., 1968, *Vistas Astron.*, 10, 125
- Fletcher L. et al., 2011, *Space Sci. Rev.*, 159, 19
- Forbes T. G., 1988, *Sol. Phys.*, 117, 97
- Grechnev V. V., Uralov A. M., Chertok I. M., Kuzmenko I. V., Afanasyev A. N., Meshalkina N. S., Kalashnikov S. S., Kubo Y., 2011, *Sol. Phys.*, 273, 433
- Grigis P. C., Benz A. O., *ApJ*, 625, L143
- Gyórfi L., Baranyi T., Ludmány A., 2011, in Choudhary D., Strassmeier K., eds, *Proc. IAU Symp. 273, The Physics of Sun and Star Spots*. Cambridge Univ. Press, Cambridge, p. 403
- Hagyard M. J., Teuber D., West E. A., Smith J. B., 1984, *Sol. Phys.*, 91, 115
- Hannah I. G., Christe S., Krucker S., Hurford G. J., Hudson H. S., Lin R. P., 2008, *ApJ*, 677, 704
- Hannah I. G., Hudson H. S., Battaglia M., Christe S., Kašparová J., Krucker S., Kundu M. R., Veronig A., 2011, *Space Sci. Rev.*, 159, 263
- Hurford G. J. et al., 2002, *Sol. Phys.*, 210, 61
- Inglis A. R., Dennis B. R., 2012, *ApJ*, 748, 139
- Isobe T., Feigelson E. D., Akritas M. G., Babu G. J., 1990, *ApJ*, 364, 105
- Jiang Y., Bi Y., Yang J., Zheng R., Wang J., 2009, *Res. Astron. Astrophys.*, 9, 603
- Joshi B., Kushwaha U., Cho K.-S., Veronig A. M., 2013, *ApJ*, 771, 1
- Kim S., Moon Y.-J., Kim Y.-H., Park Y.-D., Kim K.-S., Choe G. S., Kim K.-H., 2008, *ApJ*, 683, 510
- Kosovichev A. G., Zharkova V., 1998, *Nature*, 393, 317
- Kubo Y., 2008, *Sol. Phys.*, 248, 85
- Kumar P., Innes D. E., 2013, *Sol. Phys.*, 288, 255
- Lin R. P. et al., 2002, *Sol. Phys.*, 210, 3
- Liu C., Lee J., Karlicky M., Choudhary D.P., Deng N., Wang H.: 2009, *ApJ*, 703, 757
- McKee C. F., Ostriker J. P., 1977, *ApJ*, 218, 148
- Magdalenic J., Marqué C., Zhukov A.N., Vršnak B., Veronig A.: 2012, *ApJ*, 746, 152
- Moon Y.-J., Choe G. S., Park Y. D., Wang H., Gallagher P. T., Chae J., Yun H. S., Goode P. R., 2002, *ApJ*, 574, 434
- Moradi H., Donea A.-C., Lindsey C., Besliu-Ionescu D., Cally P. S., 2007, *MNRAS*, 374, 1155
- Moreton G. E., Ramsey H. E., 1960, *PASP*, 72, 357
- Moretti P. F., Berrilli F., Sebastianelli A., Briand C., Pietropaolo E., 2003, *ApJ*, 589, L109
- Odstrčil D., Karlický M., 1997, *A&A*, 326, 1252
- Priest E. R., Forbes T. G., 2002, *A&AR*, 10, 313
- Sakai J. I., Kawata T., Yoshida K., Furusawa K., Cramer N. F., 2000, *ApJ*, 537, 1063
- Shibata K., Magara T., 2011, *Living Rev. Sol. Phys.*, 8, 6
- Sedov L. I., 1946, *Prikl. Mat. Mekh.*, 10, 241
- Taylor G. I., 1950, *Proc. R. Soc. A*, 201, 159
- Tenorio-Tagle G., Bodenheimer P., 1988, *ARA&A*, 26, 145
- Török T., Panasenco O., Titov V. S., Mikić Z., Reeves K. K., Velli M., Linker J. A., De Toma G., 2011, *ApJ*, 739, L63
- Yang Y.-H., Cheng C. Z., Krucker S., Lin R. P., Ip W. H., 2009, *AJ*, 693, 132
- Vršnak B., Cliver E. W., 2008, *Sol. Phys.*, 253, 215
- Wheatland M. S., 2000, *ApJ*, 536, L109
- Wheatland M. S., 2009, *Sol. Phys.*, 255, 211
- Wheatland M. S., Craig I. J. D., 2006, *Sol. Phys.*, 238, 73
- Wheeler J. C., 2012, *Phil. Trans. R. Soc. A*, 370, pp. 774-799
- Zuccarello F. et al., 2009, *A&A*, 493, 629

APPENDIX A: SPATIOTEMPORAL DISTRIBUTION OF SUCCEEDING FLARES

In this appendix, we show a collection of scatter plots representing the distribution of the succeeding flares in the $\{\log_{10}(ds); \log_{10}(dT)\}$ planes observed in the 6–12 keV energy channel and in different phases of the solar cycle.

The large scatter of the data can be explained by the observed spatial distribution of flares. It has long been known that solar flares tend to occur along magnetic polarity inversion lines (PILs), which are places favourable for repeated flaring (e.g. Hagyard et al. 1984). If there is one PIL in an AR, this means that the most probable position of the next flare close in time is in the vicinity of the previous one. If there are several PILs in the AR, the next flare may happen at a different PIL, thus the spatial distances can have a large scatter in these cases. In our large statistics of flares, these two facts will cause a log-normal distribution of spatial distances. This explains that the $\log_{10}(ds)$ data have a large scatter ranging from the spatial resolution of the *RHESSI* observations to the size of the large sunspot groups. The Shapiro–Wilk test shows that we can accept the assumption of normal distribution of $\log_{10}(ds)$ in the following intervals of $\log_{10}(dT)$: 2–2.5, 2.5–3, 3–3.5, 3.5–4. This supports the assumption of log-normal distribution of spatial distances in the case of time difference smaller than about 2–3 h. In the case of larger time differences, the evolution of sunspot groups seems to cause such changes in the position of places favourable for flaring that the probability of small spatial differences decreases. This somewhat decreases the scatter of data points but it results in the rejection of the normal distribution of $\log_{10}(ds)$.

Because of this large scatter of the data, the PCA regression gives a more reliable result than the ordinary least-squares method. By definition the first principal component (PC) represents the maximum variance among the linear combinations of the observed variables. This PC defines a direction which gives correctly the trend and its slope of the point pattern in the plain of the observed variables. In contrast, the ordinary least-squares method systematically underestimates the value of this slope if both the observed variables contain a stochastic noise term (see, e.g. Deeming 1968 for the study of the role of the PCA in astronomical context).

We have made a compromise between the resolution according to the phase of the solar activity cycle and the accuracy of determining the statistical parameters of the sub-samples. To ensure the same numbers of points (1800) in these scatter plots, the time intervals corresponding to the different figures are different. Note the remarkable homogeneity of the distributions independently of time. The chi-square test based on the data in Table 2 shows that the variations of a and b are not significant. The result of chi-square test is similar if the data set is divided into six sub-intervals with equal length of one and a half year. This means that the parameters a and b can be reckoned as constants. This homogeneity of the parameters of the fitted lines makes serious restrictions for the models trying to provide with a theoretical explanation: the parameters responsible for this effect should be independent of the actual phase of the solar activity cycle.

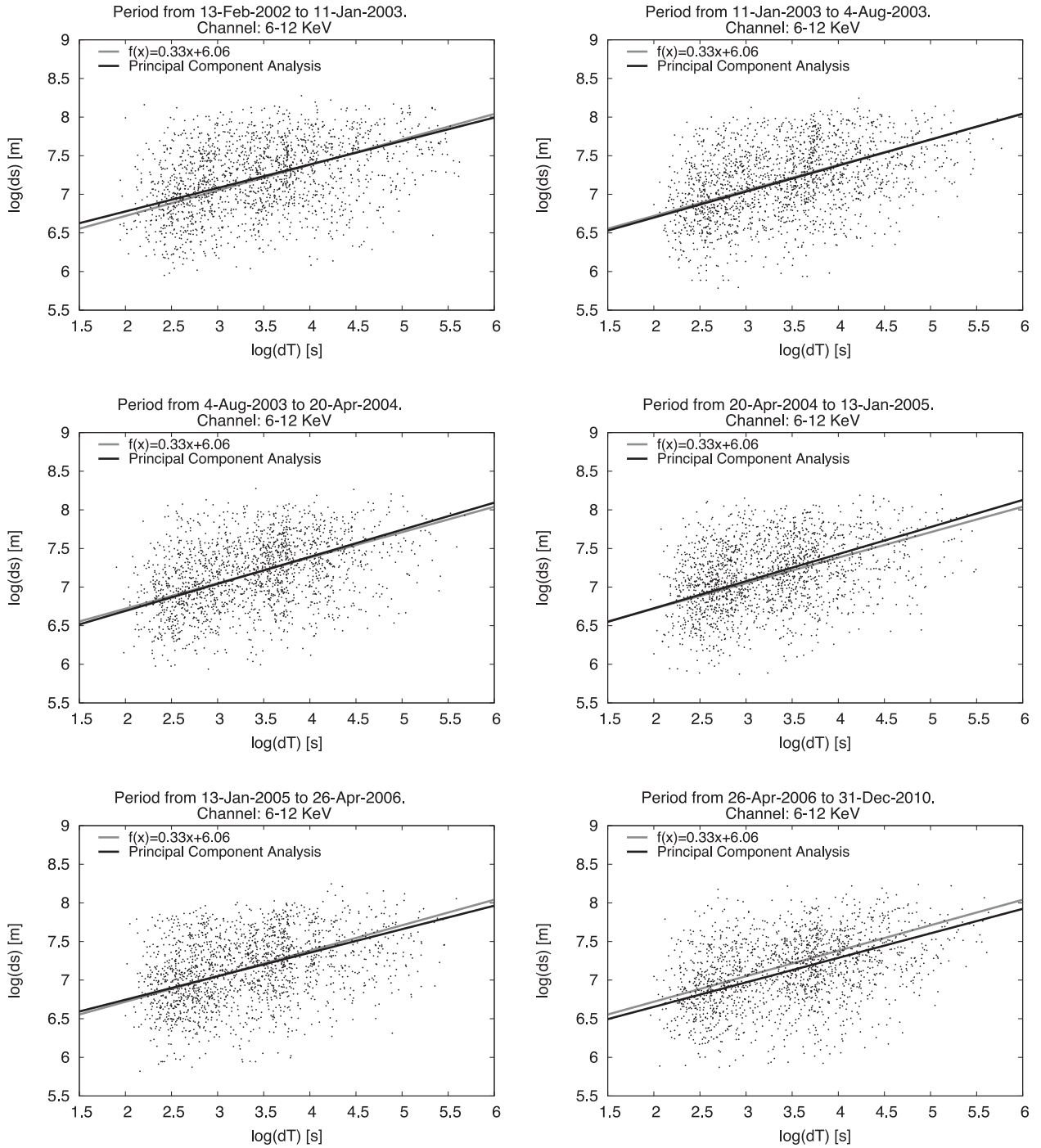


Figure A1. Distribution of flares measured in the 6–12 keV channel and their successors in the $\{\log_{10}(ds); \log_{10}(dT)\}$ plane. The black solid line indicates the actual result of the PCA regression and the grey line is determined by the average parameters in Table 2.

This paper has been typeset from a $\text{\TeX}/\text{\LaTeX}$ file prepared by the author.